Supporting Information

Sato *et al.* 10.1073/pnas.0812261106

SI Text

Comparison of Sequences of γ-secretase Substrates. The Notch signaling protein (1–3), Cd44 (4), ErbB4 (5, 6), and N-cadherin (1) are cleaved by γ-secretase *in vivo* (Fig. S1). These γ-secretase substrates are all cleaved near the TM-JM boundary. However, only Notch and Cd44 are also cleaved in the middle of the TM domain. The sequences are not conserved. Notch1 is cleaved at Ala-1,731 (S4 site) in the TM domain (2) and at Gly-1,743 (S3 site) at the TM-JM boundary (3). Similar to APP, ErbB4 has several glycine residues in the N-terminal portion of the TM domain, while N-cadherin has a significant number of β-branched isoleucine residues within its TM domain. In contrast, the TM sequences of Notch1 and CD44 consist largely of non β-branched amino acids.

One common element between the various γ-secretase substrates is that the TM region is terminated by a series of basic amino acids. We show here that in APP and Notch1 there is a helix-to-coil transition at the TM-JM boundary. The observation that APP and Notch1 can compete for γ-secretase activity suggests that this common structural feature is related to proteolysis (7–9).

ErbB4 is in the ErbB family of receptor tyrosine kinases (Fig. S1). Similar to both APP and Notch1, the ErbB4 TM domain has a propensity to dimerize in membranes (10). The N-terminal TM sequence of ErbB4 contains a GxxxG motif that may facilitate dimerization as in APP. Moreover, we have shown the TM domain of the ErbB1 receptor is α-helical and there is a break in helical structure at the TM-JM boundary (11).

Progressive Cleavage Mechanism of Proteolysis.

We propose that the helical secondary structure is maintained for all of the γ-secretase substrates within the middle of the TM domain and that the helix breaks near the ε-cut site at the TM-JM boundary. This helix-to-coil transition is required for γ-secretase processing. The 3L APP mutation, which extends the TM α-helix, inhibits ε cleavage and leads to a low production of Aβ peptides and an accumulation of the α- and β-C-terminal fragments. These data support a progressive cleavage mechanism for APP proteolysis that depends on the helix-to-coil transition at the TM-JM boundary and unraveling of the TM α-helix (Fig. S2).

One of the first indications that the γ-secretase complex was able to cleave APP between the γ- and ε-cut sites was the isolation of Aβ46 peptides (12). More recently, additional Aβ peptides have been detected with lengths intermediate between Aβ49 (ε cleavage) and Aβ42 (γ cleavage) (13–15). For example, Qi-Takahara *et al.* (13) found that the DAPT inhibitor, which suppresses Aβ40, builds up Aβ43 and Aβ46 intracellularly. They proposed an α-helical model in which the APP is cleaved at every three residues in a progressive fashion. The presence of three hydrophobic amino acids between the ε-cut site and the series of charged basic residues at the TM-JM boundary suggests that there may be a binding pocket on the γ-secretase complex that positions the bond to be cleaved.

Mutation of residues between the γ- and ε-cut sites has also provided evidence for a progressive cleavage mechanism. Replacement of residues corresponding to the γ-cut site with tryptophan resulted in Aβ peptides longer than 43 residues, whereas replacement of residues corresponding to the ε-cut site with tryptophan blocks all production of Aβ peptides (16). Replacement of residues between the γ- and ε-cut sites (i.e., positions 43 and 52) with phenylalanine all resulted in a decrease in total Aβ peptide production (17), with the largest effects being seen at intervals of 3 aa (i.e., at positions 43, 48, and 51).

We illustrate a model for the progressive cleavage mechanism in Fig. S2. The charged KKK sequence at the C-terminal end of the TM domain is unstructured and is most likely solvent exposed. The last three hydrophobic amino acids in the TM sequence (VML) would conceivably bind to a hydrophobic pocket in the γ-secretase complex adjacent to the active site aspartic acids. Cleavage at the Leu-645-Val-646 bond creates the Aβ49 peptide with a charged C terminus. The peptide is either released from the γ-secretase complex or unravels with the charged C terminus shifting to the position previously occupied by Lys-649. The Val-642-Ile-643 bond is now positioned in the enzyme active site where cleavage releases the Aβ46 peptide. At this stage, the shift of three amino acids would generate Aβ43 and then Aβ40, whereas a shift of four amino acids would generate Aβ42. These four amino acids (highlighted in blue) correspond to the four FAD sites in cluster 2 within the TM domain, that is, Thr-639, Val-640, Ile-641, and Val-642. The model suggests that the FAD mutations are responsible for this shift of four amino acids, rather than three, after the cleavage to form Aβ46. In support of this model are mutations after the ε-cut site [K649N (18) and L648P (19)], which results in an increase in the Aβ42/Aβ40 ratio. After the enzyme has cleaved to the position of Ala-638 (Aβ42) or Val-636 (Aβ40), the Aβ peptide partitions out of the bilayer and is secreted into the extracellular environment.

Implications of the Structural Model of the APP TM Dimer on γ-secretase Processing.

The sequences of γ-secretase substrates and many of the mutational studies undertaken to date support the progressive cleavage mechanism of γ-secretase processing. Although a complete understanding of the mechanism of intramembraneous proteolysis of APP will not be possible until high resolution structures are available of C99 (and its mutants) bound to the γ-secretase complex, the APP TM dimer structure presented here provides a framework for further structure-function correlations.

For example, there are two clusters of FAD mutations in the APP sequence. The first cluster is within the extracellular JM sequence and includes residues Ala-617-Glu-618-Asp-619. The Flemish mutation, where Ala-617 is replaced by glycine, results in a fourth consecutive GxxxG motif in the APP sequence. The structural consequence of this mutation is not clear and may depend on whether this region is structured and the amino acid at position 617 is accessible to water. Glycine is typically a helix breaker in soluble proteins; glycine is conformationally flexible and consequently a helix-to-coil transition is entropically favored if water is available to solvate the polar backbone C = O and NH groups. (Glycines are well-tolerated in hydrophobic environments because intramolecular hydrogen bonding of the backbone C = O and NH groups is enthalpically favored in the absence of water.) The additional GxxxG motif created by the A671G mutation encompasses the polar Glu-618-Asp-619 sequence and is thought to be located outside of the membrane. However, a recent solution NMR study in detergent micelles suggests that the amino acids just N-terminal to Ala-617 (i.e., Leu-613-Val-614-Phe-615-Phe-616) are buried within the hydrophobic interior of the micelle and not accessible to water (20).

The NMR studies on the GxxxG motifs reported here provide a framework to address the structural changes involved in the Flemish mutation both in APP and in Aβ peptides. The backbone $^{13}C = O$ and $^{13}C\alpha$ chemical shifts are sensitive to secondary structure. We typically observe $^{13}C\alpha$ chemical shifts in the range of 44–46 ppm for glycines in α-helices and less than 43 ppm for

glycines in extended β-structure. The observed chemical shifts of Gly-625 (44.6 ppm), Gly-629 (44.9 ppm), Gly-633 (44.6 ppm), and Gly-634 (45.4 ppm) are similar and significantly higher than the chemical shift of the JM glycine in Notch1 (Gly-1,755, 42.5 ppm) (see Fig. S3). The $^{13}C\alpha$ chemical shifts of Gly-33 and Gly-37 in amyloid fibrils of Aβ42, generated from cleavage of APP, are at 41.7 and 42.5 ppm, respectively. Structural studies are in progress to determine whether Gly-617 in the APP TM dimer is water-exposed and serves to break the TM dimer at the membrane surface or is not accessible to water and extends the TM dimer on the extracellular side of the membrane by facilitating helix-helix contacts.

The second cluster of FAD mutants occurs within the TM domain of APP between the γ-and ε-cut sites. Gorman *et al.* (21) using FAD mutants found that increased dimerization can reduce the Aβ42/Aβ40 ratio. They proposed a model in which monomer formation leads to exposure of the backbone carbonyl of Ala-638, the γ-cut site responsible for the production of Aβ42. The FAD mutations in the TM cluster include T639I (22), V640M (23), I641V (24), and V642I (25). In the dimer structure presented here, Val-640 and Ile-641 have contacts within the dimer interface, whereas Thr-639 and Val-642 face away from the interface. Consequently, it remains unclear how the FAD mutations would disrupt dimerization at these noninterfacial positions. Structural studies showing the effect of the FAD mutations on local secondary structure and dynamics of the APP TM helix, as well as on the propensity for dimerization, will be needed to fully address the mechanism for how the FAD mutations increase the Aβ42/Aβ40 ratio.

A third region of the APP sequence that influences APP processing is the cytoplasmic C-terminal tail. The structure of the C-terminal tail, phosphorylation at Thr-668 and binding of cytoplasmic proteins are all likely involved in regulating ε-cleavage (26–28). The above data indicate that there is a break in helical secondary structure near the ε-cut site at the TM-JM boundary. To determine whether the break in the helix is a partial unwinding around the ε-cut site or if the JM region has nonhelical secondary structure, we obtained CD spectra and NMR spectra of isolated JM peptides in solution and with membrane bicelles. Solution NMR studies have previously shown that the N-terminal residues of the isolated JM domain of APP are unstructured (29, 30). However, it is known that binding of unstructured amphipathic sequences to the membranes can nucleate helical secondary structure. CD measurements (Fig. S4) and ^1H MAS NOESY experiments (data not shown) undertaken here indicate that the presence of the membrane bilayer does not influence the unstructured JM domain. Nevertheless, it remains an open question as to whether the C-terminal tail interacts with membrane bilayers either directly as suggested by a recent solution NMR study (20) or by binding to membrane-associated proteins, such as Dab2, a PI(4,5)P$_2$ binding protein (27). Structural studies of the APP TM dimer with the full cytoplasmic sequence will be needed in the presence of cytoplasmic proteins known to bind to the APP C terminus to fully address how APP processing is regulated.

Computational Searches. The observation that the TM domain is α-helical and is able to homodimerize provides the basis for computational studies to define likely helix-helix contacts. The three variables in the search are the helix crossing angle, the axial separation between helices and the rotational angle along the helix axis (φ_1 and φ_2) for each monomer. TM helices typically associate with either left-handed or right-handed crossing angles, the axial separation at the helix crossing point ranges from approximately 8.5 to 10.5 Å and, in a full search, the helices can have any rotation angle between 0° and 360°. The strategy is to identify possible low energy dimer structures and to evaluate these structures on the basis of mutational analysis and/or
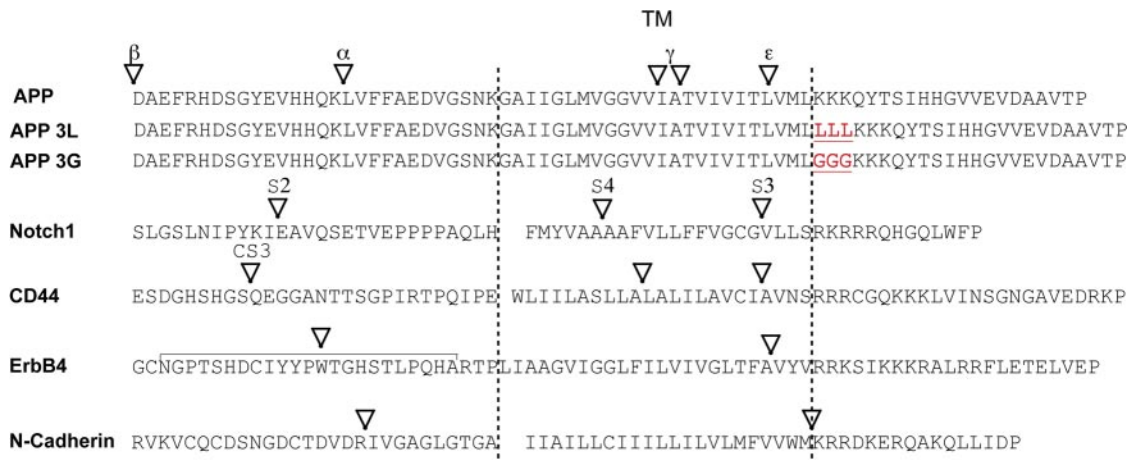
structural measurements. We have previously used this approach to generate and identify low energy TM helix dimer structures of glycophorin A (31), the Neu receptor (32), and gp55-P (33) consistent with structural constraints derived from solid-state NMR. The interhelical solid-state NMR contacts are not used as input for guiding or constraining the simulations.

To search the range of possible dimer structures, the computational search program CHI developed by Adams and Brünger (34, 35) sets up grids for both left- and right-handed dimers. For each grid, low-energy conformations of helix dimers are obtained by rotating each helix through rotation angles φ_1 and φ_2 from 0° to 360° with a sampling step size of 25–45°. (The φ_1 and φ_2 angles are equivalent to the α and β angles originally described by Adams *et al.* (34).) Separate calculations are performed for different interhelical separations. We typically compare the results for searches with interhelical separations of 8.5 Å, 9.0 Å, 9.5 Å, 10.0 Å, and 10.5 Å. MD simulations are run with simulated annealing at each rotational orientation of the dimer using the program X-PLOR along with the united atom topology and parameters sets, TOPH19 and PARAM19, respectively. For both left- and right-handed geometries, the initial crossing angles are set at 25°. The rotation and crossing angles are allowed to vary during the simulations, whereas the interhelical separation is fixed. To maintain an α-helical conformation, distance restraints are applied between O_i and $N_{i + 4}$ atoms along the backbone. Following the MD simulations and energy minimization, the various structures within the search grid are compared by cluster analysis. Dimer structures with similar structures are defined as a cluster if their root mean square difference is less than 1 Å. The clusters are first evaluated in terms of the number of individual dimer structures. The individual structures are then averaged and energy minimized for each cluster to give a single representative dimer structure. These structures can be compared on the basis of their energy and whether they are observed at different interhelical separations. The most robust low energy structures appear in computational searches using a range of interhelical separations (i.e., they show up in more than a single search).

Fig. S5 presents the cluster analysis for one computational search using an interhelical separation of 9.5 Å. For this search, APP helices were formed using residues 625–648. In total, 22 clusters of structures were observed, 11 right-handed clusters and 11 left-handed clusters. Two right-handed clusters (clusters 17 and 22) were observed along the diagonal in Fig. S5. There were no symmetric clusters in the parallel search of dimers with left-handed crossing angles. The two symmetric clusters with right-handed crossing angles have either the GxxxG sequences (cluster 17) or GxxxA sequence (cluster 22) oriented toward the dimer interface. Two clusters are observed with a φ_1 angle of approximately 350° and a φ_2 angle of approximately 200° and 100°. These correspond to dimer structures where only one of the two helices in the dimer is oriented with the consecutive GxxxG sequences facing into the interface. Similarly, four clusters are observed with a φ_2 angle of approximately 350° and a φ_1 angle of approximately 25°, 90°, 100°, and 200°. These results are in agreement with the general ability of GxxxG sequences to mediate dimerization.

We observe clusters similar to cluster 17 in the computational searches where the interhelical distances are set at 8.5 Å, 9.0 Å, 9.5 Å, and 10 Å, and clusters similar to cluster 22 at interhelical distances of 8.5 Å, 9.0 Å, and 9.5 Å. However, we do not observe these clusters with longer axial separations, consistent with the close helix-helix packing mediated by the GxxxG and GxxxA sequences. The search shown in Fig. S5 was carried out on APP helices formed using residues 625–648, which includes the two C-terminal GxxxGxxxG motifs. Similar results are observed for computational searches with longer stretches of the APP sequence (residues 621–648), which includes all three consecutive GxxxG motifs.

1. Marambaud P, *et al.* (2002) A presenilin-1/γ-secretase cleavage releases the E-cadherin intracellular domain and regulates disassembly of adherens junctions. *EMBO J* 21:1948–1956.
2. Okochi M, *et al.* (2002) Presenilins mediate a dual intramembranous gamma-secretase cleavage of Notch-1. *EMBO J* 21:5408–5416.
3. Schroeter EH, Kisslinger JA, Kopan R (1998) Notch-1 signalling requires ligand-induced proteolytic release of intracellular domain. *Nature* 393:382–386.
4. Lammich S, *et al.* (2002) Presenilin-dependent intramembrane proteolysis of CD44 leads to the liberation of its intracellular domain and the secretion of an Aβ-like peptide. *J Biol Chem* 277:44754–44759.
5. Lee HJ, *et al.* (2002) Presenilin-dependent γ-secretase-like intramembrane cleavage of ErbB4. *J Biol Chem* 277:6318–6323.
6. Vidal GA, Naresh A, Marrero L, Jones FE (2005) Presenilin-dependent γ-secretase processing regulates multiple ERBB4/HER4 activities. *J Biol Chem* 280:19777–19783.
7. Lewis HD, *et al.* (2003) Catalytic site-directed gamma-secretase complex inhibitors do not discriminate pharmacologically between notch S3 and beta-APP cleavages. *Biochemistry* 42:7580–7586.
8. Berezovska O, *et al.* (2001) Notch1 and amyloid precursor protein are competitive substrates for presenilin1-dependent gamma-secretase cleavage. *J Biol Chem* 276:30018–30023.
9. Lleo A, *et al.* (2003) Notch1 competes with the amyloid precursor protein for gamma-secretase and down-regulates presenilin-1 gene expression. *J Biol Chem* 278:47370–47375.
10. Duneau JP, Vegh AP, Sturgis JN (2007) A dimerization hierarchy in the transmembrane domains of the HER receptor family. *Biochemistry* 46:2010–2019.
11. Sato T, Pallavi P, Golebiewska U, McLaughlin S, Smith SO (2006) Structure of the membrane reconstituted transmembrane-juxtamembrane peptide EGFR(622–660) and its interaction with Ca2+/calmodulin. *Biochemistry* 45:12704–12714.
12. Yu CJ, *et al.* (2001) Characterization of a presenilin-mediated amyloid precursor protein carboxyl-terminal fragment gamma - Evidence for distinct mechanisms involved in gamma-secretase processing or the APP and Notch1 transmembrane domains. *J Biol Chem* 276:43756–43760.
13. Qi-Takahara Y, *et al.* (2005) Longer forms of amyloid β protein: implications for the mechanism of intramembrane cleavage by gamma-secretase. *J Neurosci* 25:436–445.
14. Yagishita S, Morishima-Kawashima M, Tanimura Y, Ishiura S, Ihara Y (2006) DAPT-induced intracellular accumulations of longer amyloid β-proteins: Further implications for the mechanism of intramembrane cleavage by γ-secretase. *Biochemistry* 45:3952–3960.
15. Zhao GJ, *et al.* (2005) γ-cleavage is dependent on ζ-cleavage during the proteolytic processing of amyloid precursor protein within its transmembrane domain. *J Biol Chem* 280:37689–37697.
16. Sato T, *et al.* (2005) Blocking the cleavage at midportion between γ- and ε-sites remarkably suppresses the generation of amyloid β-protein. *FEBS Lett* 579:2907–2912.
17. Tan J, *et al.* (2008) Effects of gamma-secretase cleavage-region mutations on APP processing and Abeta formation: interpretation with sequential cleavage and alpha-helical model. *J Neurochem* doi: 10.1111/j. 1471–4159.2008.05643.x

18. Theuns J, *et al.* (2006) Alzheimer dementia caused by a novel mutation located in the APP C-terminal intracytosolic fragment. *Hum Mutat* 27:888–896.
19. Tesco G, *et al.* (2005) APP substitutions V715F and L720P alter PS1 conformation and differentially affect Aβ and AICD generation. *J Neurochem* 95:446–456.
20. Beel AJ, *et al.* (2008) Structural studies of the transmembrane C-terminal domain of the amyloid precursor protein (APP): Does APP function as a cholesterol sensor? *Biochemistry* 47:9428–9446.
21. Gorman PM, *et al.* (2008) Dimerization of the transmembrane domain of amyloid precursor proteins and familial Alzheimer's disease mutants. *BMC Neuroscience* 9:17.
22. Kumar-Singh S, *et al.* (2000) Nonfibrillar diffuse amyloid deposition due to a γ42-secretase site mutation points to an essential role for N-truncated Aβ42 in Alzheimer's disease. *Hum Mol Genet* 9:2589–2598.
23. Ancolio K, *et al.* (1999) Unusual phenotypic alteration of β amyloid precursor protein (β APP) maturation by a new Val-715 -> Met beta APP-770 mutation responsible for probable early-onset Alzheimer's disease. *Proc Natl Acad Sci USA* 96:4119–4124.
24. Eckman CB, *et al.* (1997) A new pathogenic mutation in the APP gene (1716V) increases the relative proportion of Aβ42(43). *Hum Mol Genet* 6:2087–2089.
25. Mullan M, *et al.* (1993) Clinical comparison of Alzheimers-disease in pedigrees with the codon-717 Val- Ile mutation in the amyloid precursor protein gene. *Neurobiol Aging* 14:407–419.
26. Elenius K, *et al.* (1997) A novel juxtamembrane domain isoform of HER4/ErbB4. *J Biol Chem* 272:26761–26768.
27. Kerr ML, Small DH (2003) Cytoplasmic domain of the b-amyloid protein precursor of Alzheimer's disease: function, regulation of proteolysis, and implications for drug development. *J Neurosci Res* 80:151–159.
28. Lee MS, *et al.* (2003) APP processing is regulated by cytoplasmic phosphorylation. *J Cell Biol* 163:83–95.
29. Ramelot TA, Gentile LN, Nicholson LK (2000) Transient structure of the amyloid precursor protein cytoplasmic tail indicates preordering of structure for binding to cytosolic factors. *Biochemistry* 39:2714–2725.
30. Theresa A, Ramelot TA, Nicholson LK (2001) Phosphorylation-induced structural changes in the amyloid precursor protein cytoplasmic tail detected by NMR. *J Mol Biol* 307:871–884.
31. Smith SO, *et al.* (2001) Structure of the transmembrane dimer interface of glycophorin A in membrane bilayers. *Biochemistry* 40:6553–6558.
32. Smith SO, *et al.* (2002) Transmembrane interactions in the activation of the Neu receptor tyrosine kinase. *Biochemistry* 41:9321–9332.
33. Liu W, Crocker E, Constantinescu SN, Smith SO (2005) Helix packing and orientation in the transmembrane dimer of gp55-P of the spleen focus forming virus. *Biophys J* 89:1194–1202.
34. Adams PD, Arkin IT, Engelman DM, Brünger AT (1995) Computational searching and mutagenesis suggest a structure for the pentameric transmembrane domain of phospholamban. *Nat Struct Biol* 2:154–162.
35. Adams PD, Engelman DM, Brünger AT (1996) Improved prediction for the structure of the dimeric transmembrane domain of glycophorin A obtained through global searching. *Proteins* 26:257–261.

TM

```
              β                    α                    γ            ε
              ▽                    ▽                    ▽▽           ▽
APP       DAEFRHDSGYEVHHQKLVFFAEDVGSNK GAIIGLMVGGVVIATVIVITLVML KKKQYTSIHHGVVEVDAAVTP
APP 3L    DAEFRHDSGYEVHHQKLVFFAEDVGSNK GAIIGLMVGGVVIATVIVITLVML LLL KKKQYTSIHHGVVEVDAAVTP
APP 3G    DAEFRHDSGYEVHHQKLVFFAEDVGSNK GAIIGLMVGGVVIATVIVITLVML GGG KKKQYTSIHHGVVEVDAAVTP

                   S2                    S4          S3
                   ▽                     ▽           ▽
Notch1    SLGSLNIPYKIEAVQSETVEPPPPAQLH FMYVAAAAFVLLFFVGCGVLLS RKRRRQHGQLWFP

              CS3
              ▽                              ▽           ▽
CD44      ESDGHSHGSQEGGANTTSGPIRTPQIPE WLIILASLLALALILAVCIAVNS RRCGQKKKLVINSGNGAVEDRKP

                            ▽                                    ▽
ErbB4     GCNGPTSHDCIYYPWTGHSTLPQHARTP LIAAGVIGGLFILVIVGLTFAVYV RRKSIKKKRALRRFLETELVEP

                              ▽                                 ▽
N-Cadherin RVKVCQCDSNGDCTDVDRIVGAGLGTGA IIAILLCIIILLILVLMFVVWM KRRDKERQAKQLLIDP
```

Fig. S1. Sequences of γ-secretase substrates showing the position of enzymatic cleavage. The sequences of APP 3L and APP 3G (see text) containing a three leucine insert and a three glycine insert, respectively, are also shown. Potential JM cleavage sites of ErBb4 have only been localized to the region defined by the bar (26, 36). The sequences of the TM domains are not conserved. Common features of these substrates include ectodomain shedding and the presence of a cluster of basic and hydrophobic amino acids at the TM-JM boundary.
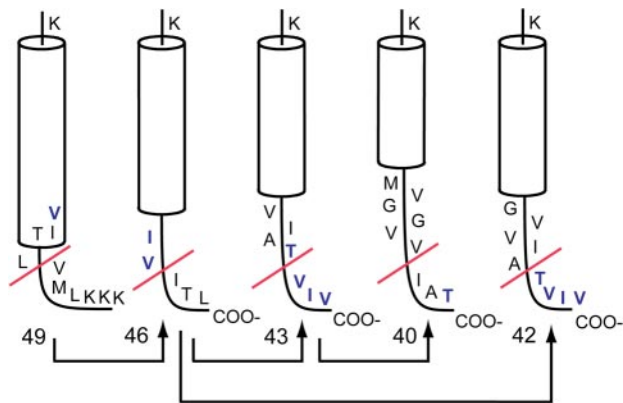
Fig. S2. The structural studies of the APP TM domain indicate that the ε-cut site is approximately 32 Å from Lys-624. Cleavage at a single site would lead to local unraveling of the helix and a shift of amino acids into the binding site. The diagram indicates that to place the Aβ42 cleavage site at the same position would result in unraveling of the TM helix to the Gly-633-Gly-634 sequence. Early onset Familial Alzheimer's Disease is caused through autosomal dominant genetic mutations on either APP or PS1. Four FAD mutations have been found between the ε- and γ-cut sites in APP: T639I (22), V640M (23), I641V (24), and V642I (25). According to the model of Qi-Takahara *et al.* (13), during the processing of Aβ40 by γ-secretase, residues 640, 641, and 642 would reside in the proposed binding pocket of γ-secretase. If any three of these residues were mutated, it would disrupt the affinity for or orientation of the substrate within the pocket.
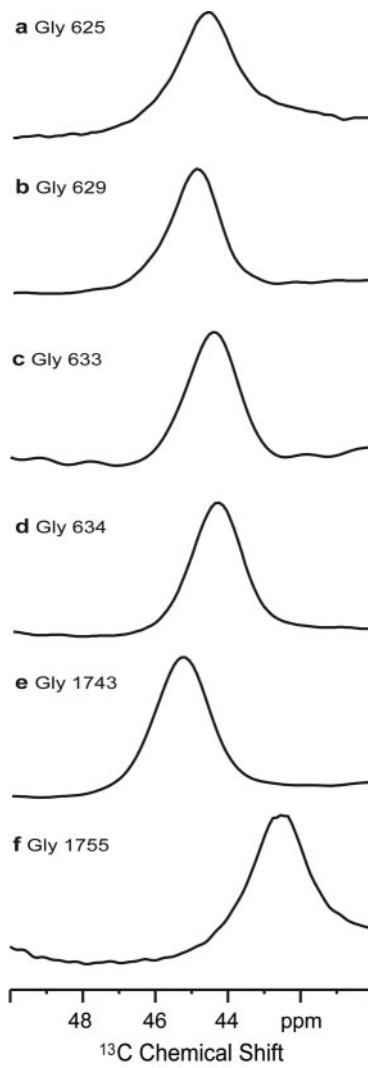
Fig. S3. ^{13}C MAS NMR APP TM-JM and Notch TM-JM peptides. MAS NMR spectra were obtained of the APP TM-JM peptide labeled with 2-^{13}C glycine at Gly-625 (*a*), Gly-629 (*b*), Gly-633 (*c*), and Gly-634 (*d*). MAS NMR spectra were obtained of the Notch TM-JM peptide labeled with 2-^{13}C glycine at Gly-1743 and Gly-1755. The molar ratio of protein-to-lipid is 1:50.
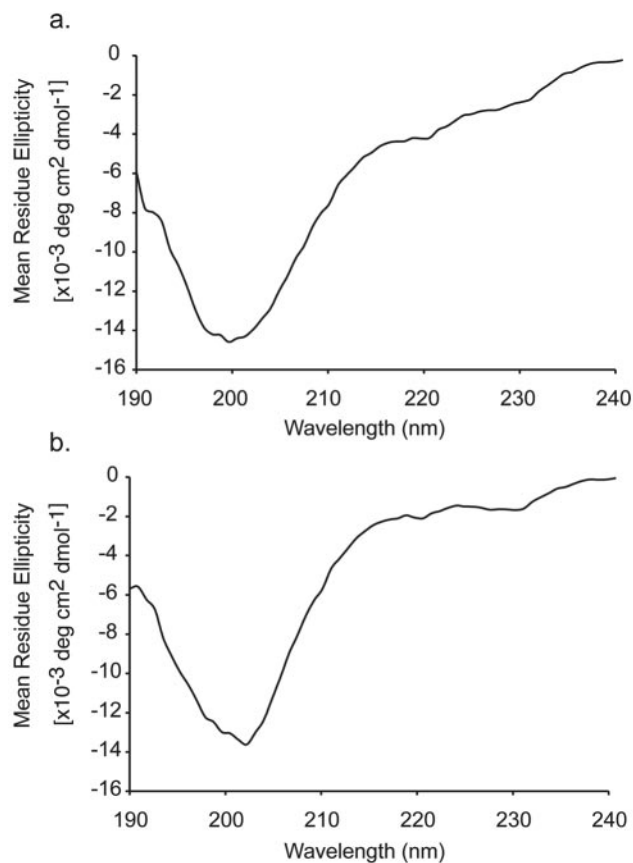
Fig. S4. CD spectra of the JM regions of APP (residues 648–672) (*a*) and Notch1 (residues 1,747–1,761) (*b*). For the JM peptides, the N terminus was acetylated. The spectra were obtained on an Olis Instruments spectrophotometer using a path length of 0.2 mm. The spectra were obtained using isotropic bicelles composed of DMPC:DMPG:DHPC in a molar ratio of 10:3:13. The total lipid concentration was 10% by volume and the peptide:lipid molar ratio was 1:100. The peptide (0.15 mg, 1.76 mmol) was added after the bicelles were formed. The samples containing DMPC and DMPG were prepared by first co-dissolving the lipids in chloroform. After removing the chloroform with a flow of argon gas, the lipids were re-dissolved in cyclohexane and lyophilized to form a fluffy powder. DHPC was separately dissolved in cyclohexane and lyophilized overnight. The DHPC powder was hydrated with 20 mM of sodium phosphate buffer (pH 6.4 at 30 °C) and the solution was subjected to five freeze-thaw cycles. The DHPC solution was then added to the lyophilized DMPC:DMPG powder. A final lipid concentration of 10% (wt/wt) was reached by diluting with sodium phosphate buffer. The solution was incubated at 38 °C for 20 min and then 4 °C for 20 min. Ten cycles of incubation were repeated to form a transparent bicelle solution.
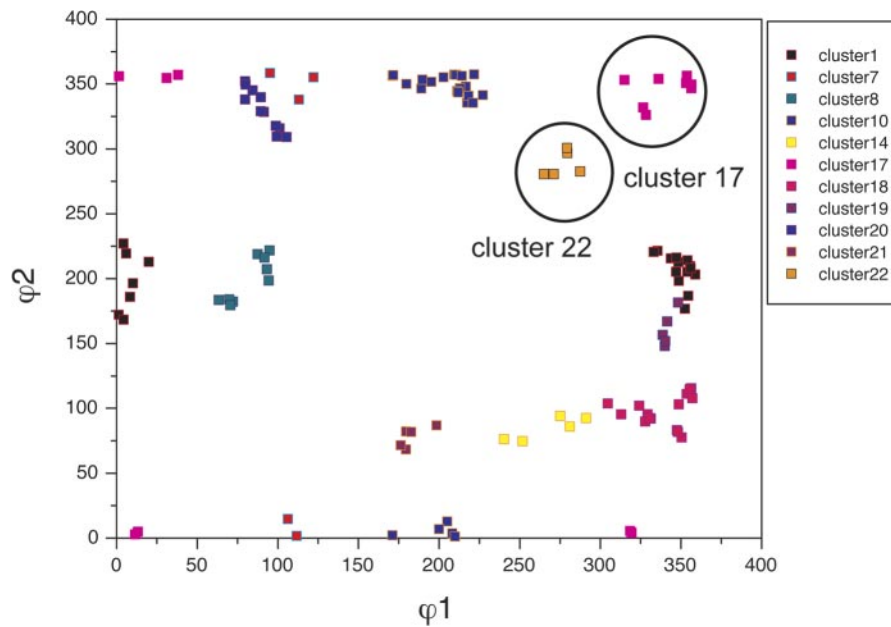
Fig. S5. Computational search for low energy dimer structures of the APP (625–648) TM domain. The search algorithm started with helix dimers having left-handed and right-handed crossing angles. The grid shown corresponds to the dimers with right-handed crossing angles. The step size for rotation was 45°. The figure plots the final φ1 and φ2 values for those structures that fall into a "cluster." A cluster is defined as a minimum of five structures with an rmsd of 1 Å or less.